IV.D.1 Design of Novel Multi-Component Metal Hydride-Based Mixtures for Hydrogen Storage

Christopher Wolverton (Primary Contact), Vidvuds Ozolins (University of California, Los Angeles), Harold H. Kung
Department of Materials Science & Engineering
Northwestern University
Evanston, IL 60208
Phone: (847) 467-0593
Email: c-wolverton@northwestern.edu

DOE Managers
Katie Randolph
Phone: (720) 356-1759
Email: Katie.Randolph@go.doe.gov
Ned Stetson
Phone: (202) 586-9995
Email: Ned.Stetson@ee.doe.gov

Subcontractors:
- Jun Yang, Ford Motor Company, Dearborn, MI
- Sheldon Shore, Ohio State University, Columbus, OH
- Sonjong Hwang, Caltech, Pasadena, CA

Contract Number: DE-FC36-08GO18136

Project Start Date: September 1, 2008
Project End Date: August 31, 2013

Overall Objectives

- Discover novel mixed hydrides for hydrogen storage which enable the DOE 2017 system-level goals.
- Discover a material that desorbs 8.5 wt% H_2 or more at temperatures below 85°C.
- Via the combination of first-principles calculations of reaction thermodynamics and kinetics with material and catalyst synthesis, testing, and characterization, search for combinations of materials from distinct categories to form novel multicomponent reactions.

Fiscal Year (FY) 2013 Objectives

- Determine storage capacities, kinetics, and reversibility for reactions predicted to have high capacity and suitable thermodynamics for H_2 storage applications, i.e., $2LiBH_4 + 5Mg(BH_4)_2$ and $B_{20}H_{16}$.
- Use combined theory and experiment to characterize reaction products from $2LiBH_4 + 5Mg(BH_4)_2$.
- Synthesize $B_{20}H_{16}$ and determine hydrogen desorption properties and reaction products.
- Develop computational methods to extend calculation of kinetics beyond mass transport to predict dissociation, surface diffusion, and other kinetic barriers.

Technical Barriers

This project addresses the following technical barriers from the Hydrogen Storage section of the Fuel Cell Technologies Office Multi-Year Research, Development, and Demonstration Plan:

(O) Lack of Understanding of Hydrogen Physisorption and Chemisorption

(A) System Weight and Volume

(E) Charging/Discharging Rates

Technical Targets

This study is aimed at fundamental insights into new materials and the thermodynamic and kinetic aspects of H_2 release and reabsorption from them. Insights gained from these studies will be applied toward the design and synthesis of hydrogen storage materials that meet the following DOE 2017 hydrogen storage targets:

- Specific energy: 1.8 kWh/kg
- Energy density: 1.3 kWh/L

FY 2013 Accomplishments

- Focused efforts on two main reactions, predicted to have high capacity and suitable thermodynamics for H_2 storage applications: $2LiBH_4 + 5Mg(BH_4)_2$ and $B_{20}H_{16}$.
- $B_{20}H_{16}$ extremely promising – first known H_2 storage reaction with high capacity, good thermodynamics, and computational predicted fast mass transport kinetics.
- Theoretically predicted that mass transport in $B_{20}H_{16}$ is fast. Subcontract at Ohio State University focused on synthesis of $B_{20}H_{16}$ compound (future plans will focus on desorption, nuclear magnetic resonance [NMR], kinetics, and reaction products – full characterization of this material).
- H_2 desorption and decomposition pathways have been studied in $2LiBH_4 + 5Mg(BH_4)_2$ using NMR; reaction products consistent with theoretically predicted B_2H_6 anion; still much to explore in this system in terms of reversibility of reaction products (see Future Plans).
- Low-temperature hydrogen desorption observed for $LiBH_4$-carbon composite. Stable cycling can be attained after a few cycles.

- Using the predictive models of kinetics of mass transport, the Al mass transport in $B_{20}H_{16}$ is quite high (important for H_2 release from AlB_4H_{11}), but the mass transport in $LiBH_4$ is very low (much lower than that in $NaAlH_4$); potential avenue for borohydrides – low-lying eutectics (see Future Plans).
- Computational survey of dopants that lower surface dissociation or diffusion for MgB_2 rehydrogenation.

INTRODUCTION

The long-term DOE targets for hydrogen storage systems are very challenging, and cannot be met with existing materials. The vast majority of the work to date has delineated materials into various classes, e.g., complex and metal hydrides, chemical hydrides, and sorbents. However, very recent studies indicate that mixtures of storage materials, particularly mixtures between various classes, hold promise to achieve technological attributes that materials within an individual class cannot reach. Our project involves a systematic, rational approach to designing novel multicomponent mixtures of materials with fast hydrogenation/dehydrogenation kinetics and favorable thermodynamics using a combination of state-of-the-art scientific computing and experimentation. Specifically, we focus on combinations of materials from distinct categories to form novel multicomponent reactions.

APPROACH

We use the accurate predictive power of first-principles modeling to understand the thermodynamic and microscopic kinetic processes involved in hydrogen release and uptake and to design new material/catalyst systems with improved properties. Detailed characterization and atomic-scale catalysis experiments elucidate the effect of dopants, and nanoscale catalysts in achieving fast kinetics and reversibility. And, state-of-the-art storage experiments give key storage attributes of the investigated reactions, validate computational predictions, and help guide and improve computational methods. In sum, our approach involves an effective blend of 1) H_2 storage measurements and characterization, 2) state-of-the-art computational modeling, 3) detailed catalysis experiments, and 4) an in-depth automotive perspective.

RESULTS (SELECTED EXAMPLES)

Fast Mass Transport Kinetics in $B_{20}H_{16}$: A High-Capacity Hydrogen Storage Material

The storage of hydrogen in an economical and practical way remains a significant challenge in the development of hydrogen fuel cell vehicles. Reversible storage in the solid state (such as in complex metal hydrides) has gained much interest due to the favorable storage densities that can be achieved. A candidate material must release hydrogen at a few bar and operate using the waste heat from the proton exchange membrane fuel cell. Well-established methods such as the grand canonical linear programming method have been used to screen hydrogen storage reactions using energetics obtained from first-principles calculations in order to determine those that are thermodynamically allowable. Besides releasing and absorbing hydrogen in the target range of temperatures and pressures, these reactions should occur rapidly where the targeted rehydrogenation rate proposed by the DOE is 2.0 kg H_2/min. Of the known hydrogen storage reactions that have thermodynamic properties and storage capacities that meet the DOE targets, all suffer from unacceptably slow reaction rates.

There are many processes that may limit the dehydrogenation or rehydrogenation rates of metal hydrides such as nucleation, growth, and H_2 dissociation and recombination at surfaces. In particular, many studies have focused on the kinetics of long-range mass transport during the growth stage. There are both experimental and theoretical evidence that this mass transport step occurs via the diffusion of point defects through bulk phases and that it may be rate limiting in many reactions. This provides motivation to determine the mass transport barrier for proposed reactions. Those reactions with high mass transport barriers can be disregarded for practical applications since their kinetics will be unacceptably slow, unless a suitable catalyst can be found.

Recently, the decomposition of $B_{20}H_{16}$ (Figure 1) has been predicted to occur via a single-step reaction:

$$B_{20}H_{16} \rightarrow 20B + 8H_2$$

The enthalpy change of reaction is equal to 33 kJ/mol H_2 with a calculated equilibrium temperature of 20°C (at a pressure of 1 bar H_2), releasing 6.9 wt% H_2 with a volumetric density of 64.1 g H_2/L. These thermodynamic properties and large storage capacity makes this reaction attractive for applications in passenger vehicles. We focus on the kinetics of mass transport in reaction.

Free energies of formation for defects are plotted versus temperature in Figure 2 at both of the interfaces inserted in Figure 2. Of the defects in $B_{20}H_{16}$, we find that interstitial H_2 has the lowest free energy of formation under all assumed conditions; it is equal to 0.55 eV/defect at the $B/B_{20}H_{16}$ interface and increases from 0.28 to 0.63 eV/defect at the $B_{20}H_{16}/H_2$ interface as the temperature is increased from 250 to 500 K. This temperature dependence of the free energy of formation is due to the chemical potential of hydrogen gas, which decreases with increasing temperature. Of the remaining defects, the formation energy of neutral BH vacancies is several hundred meV above that of interstitial

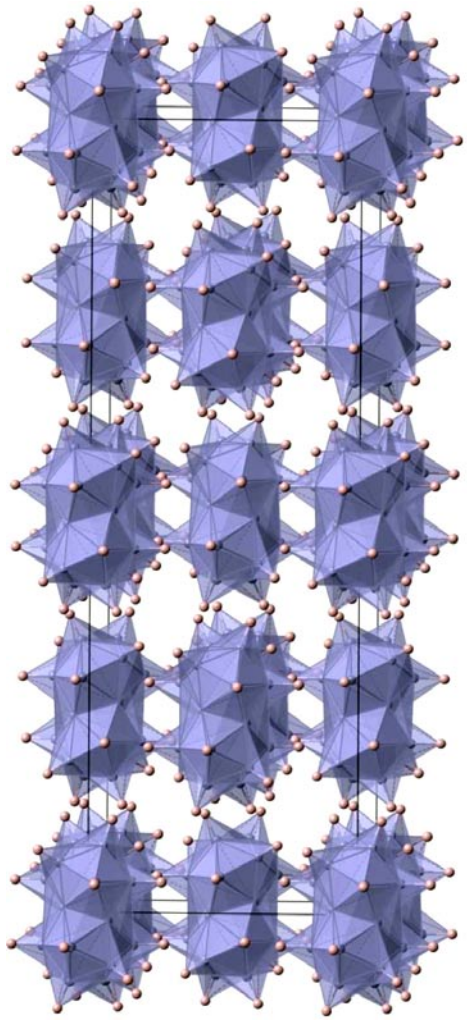

FIGURE 1. Structure of $B_{20}H_{16}$ with B atoms represented by purple spheres, H atoms by pink spheres, and $B_{20}H_{16}$ clusters by polyhedra.

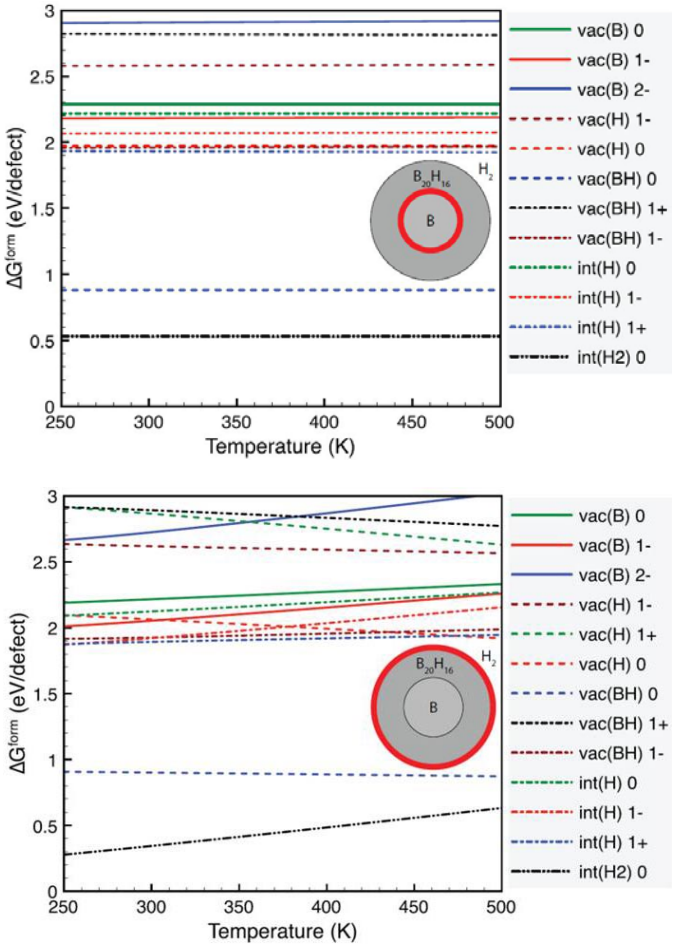

FIGURE 2. Free energies of formation for defects in $B_{20}H_{16}$. Only those defects with formation energies of less than 3 eV are shown. The bold red lines on the inset morphologies show the interfaces at which each set of formation energies is calculated.

H_2 and all other defect formation energies are still higher by at least 1 eV. From steric arguments used in most crystals, it is somewhat surprising that an H_2 dimer, instead of some other monatomic type, is the lowest-energy interstitial defect. However, since $B_{20}H_{16}$ is a molecular crystal, there exist large voids in the structure in which it is possible that both atoms in an H_2 dimer can each be more than 1.5 Å from any other atom in the crystal. This large distance between the H_2 dimer and the host $B_{20}H_{16}$ clusters allows the formation energy of this interstitial defect to remain relatively low.

Having established that interstitial H_2 forms with the lowest energy of all defects, we now turn to the diffusion of this type. From Kinetic Monte Carlo (KMC) simulations, we find that the energy landscape between interstitial H_2 sites in $B_{20}H_{16}$ is relatively flat and that the largest barrier for diffusion is only 116 meV. Using the concentration gradients obtained from the energies shown in Figure 2, and the diffusivities obtained from KMC simulations, the overall flux of interstitial H_2 is shown on an Arrhenius plot in Figure 3. Since the flux depends on the length of the region over which the concentration gradient is calculated, we have made the arbitrary choice to show the results when the length of the $B_{20}H_{16}$ region is 1 μm; however, such a choice will have no effect on the calculated activation energy since this distance does not depend on temperature. The vertical, dashed line in this figure shows the location of the equilibrium temperature for $B_{20}H_{16} \rightarrow 20B + 8H_2$, where the concentration gradient, and thus flux, decreases to zero since the chemical potential of hydrogen is exactly equal at both interfaces at this temperature. Taking the slopes above and below the critical temperature in Figure 3, we find that the activation energies for dehydrogenation and rehydrogenation are 70 and 6 kJ/mol, respectively. We note that the activation energy, especially for dehydrogenation, is lower than the free energies of formation shown in Figure 2. Therefore, the mass transport rates in reaction should be sufficiently fast for practical applications. It must be emphasized that rapid

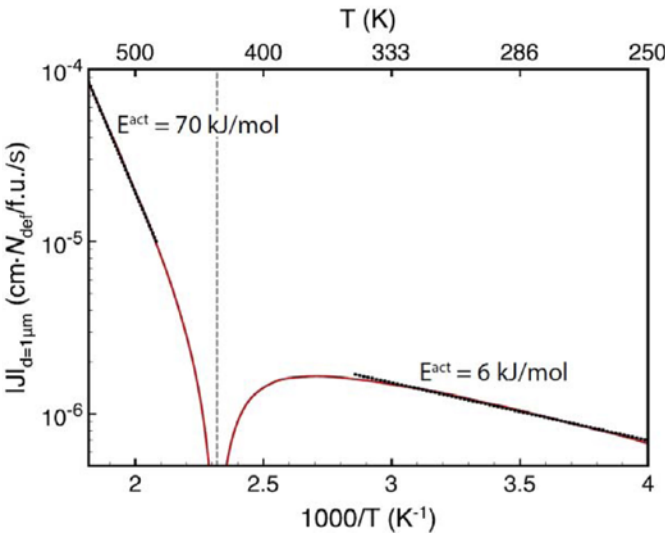

FIGURE 3. Calculated flux of interstitial H_2 across a 1-μm region of $B_{20}H_{16}$. The vertical dashed line shows the equilibrium temperature for the reaction. Separate linear fits to high- and low-temperature regions are shown as dotted black lines along with the associated activation energy.

mass transport is a necessary, but not sufficient, condition for reaction kinetics that are acceptably fast. Other processes such as nucleation and H_2 dissociation may also limit the reaction rate. However, methods for catalyzing these processes in particular have already been demonstrated in other hydrogen storage systems. With this, the combination of fast mast transport kinetics and large hydrogen content in $B_{20}H_{16}$ makes this material promising for the vehicular storage of hydrogen.

The Synthesis of Icosaborane-16 ($B_{20}H_{16}$)

Several methods have been reported for the preparation of icosaborane-16 ($B_{20}H_{16}$) but all were carried out under extreme condition and with as low as 9 to 15% yield. No commercial source is available. The method we plan to use in this project is a modified catalytic pyrolysis of decaborane-14 ($B_{10}H_{14}$). The reported yields for the original procedure range from 10 to 15%.

The synthesis of catalyst, methylaminodimethylborane

A 1:1 molar ratio of methylamine and trimethylborne were condensed in a container and then the mixture was heated 2 hours at 310ºC. The formed products after heating were then opened to traps maintained at -95°C and -196°C. The contents of the -95°C trap were distilled to produce methylaminodimethylborane. The overall procedure includes the following two reactions.

$$MeNH_2 + BMe_3 \rightarrow MeNH_2BMe_3 \quad (1)$$

$$MeNH_2BMe_3 \rightarrow MeNHBMe_2 + CH_4 \quad (2)$$

The synthesis of icosaborane-16

Decaborane-14 was charged in a container which is connected to a tube. In another container, catalyst of methylaminodimethylborane was charged and also connected to the tube. The flow rate of both chemicals can be adjusted. Daceborane-14 will be heated at 100°C and methylaminodimethylborane will kept at 0°C. Both staring materials are passed through the tube whose middle part will be heated at 350°C under dynamic vacuum. The other end of the tube connected to pump through a liquid nitrogen trap. The product will deposit just outside the hot zone of the pyrolysis tube. The raw product was purified by repeated sublimation.

Characterizing Carbon Catalysts for Mixed $LiBH_4$-$Mg(BH_4)_2$ Dehydrogenation/Rehydrogenation

We had observed better cyclability in complex metal hydride-carbon composite (~40% metal hydride loading and prepared by room temperature liquid infusion) when the hydride was $LiBH_4$as compared with the mixed $LiBH_4$-$Mg(BH_4)_2$.

Although the mixed hydride $LiBH_4$-$Mg(BH_4)_2$ had better dehydriding property than $LiBH_4$, the poor reversibility is problematic. We set out to determine whether the single hydride, $Mg(BH_4)_2$, on carbon can be rehydrided. Figure 4 shows several cycles of hydrogenation and dehydrogenation of $Mg(BH_4)_2$-carbon composite. H_2 released is expressed as wt% of the total composite and should be higher if only $Mg(BH_4)_2$was considered. The hydriding was performed at 300°C at 50-bar H_2 pressure for 15 h. The extent of rehydriding was poor compared with $LiBH_4$-carbon composite rehydrided at only 11 bar pressure for 1 h and it appeared that the amount of hydrogen released decreased with each cycle. This data seemed in line with literature reports indicating that $Mg(BH_4)_2$ can only be rehydrided under harsh conditions. The proposed cause for the continuous erosion in hydrogen storage property was the formation of $MgB_{12}H_{12}$. Stavilahas reported that $Li_2B_{12}H_{12}$ and $Na_2B_{12}H_{12}$ can be rehydrogenated at conditions that $Ca_2B_{12}H_{12}$ show no rehydrogenation. We propose that the observed difference in the reversibility of composites of carbon-$LiBH_4$ and carbon-$Mg(BH_4)_2$ is due to the difference in the ease of rehydrogenation of the products $Li_2B_{12}H_{12}$ and $MgB_{12}H_{12}$. It has been reported that the H_2 desorption pressure at 300°C in a $LiBH_4$-carbon composite prepared by melt infusion can greatly exceed that dictated by thermodynamics for the decomposition pathway of $LiBH_4$ to LiH+ B +1.5 H_2. However, if a significant fraction of $LiBH_4$ decomposed through the $Li_2B_{12}H_{12}$ ($LiBH_4 \rightarrow 10/12$ LiH + $1/12Li_2B_{12}H_{12}$ + 13/12 H_2) pathway then higher pressure is possible. The observed pressures from some of our experiments also suggest that a portion of $LiBH_4$ in the composite may decompose through the $Li_2B_{12}H_{12}$ pathway. It is not surprising

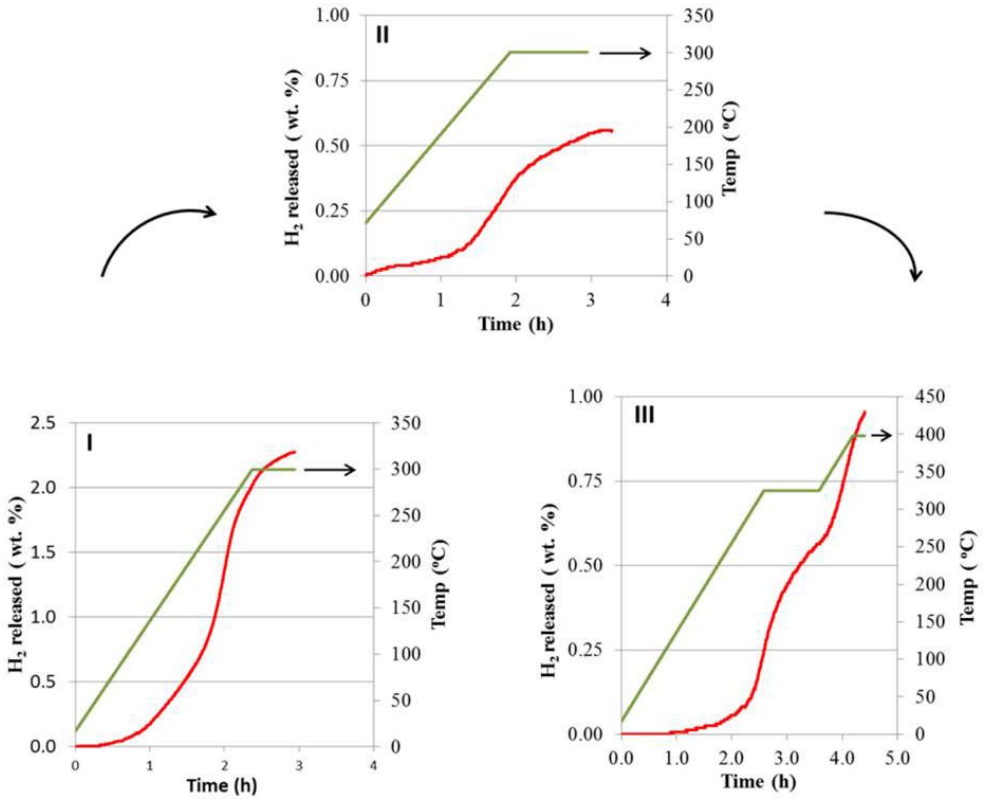

FIGURE 4. Three dehydriding cycles of $Mg(BH_4)_2$-carbon composite (hydride loading is 34.8 wt%). After each dehyriding, the sample was rehydrided for 15 h at 50-bar H_2.

that in a confined space, clustering of BH_4^- to generate $B_{12}H_{12}^=$ may be facilitated. Thus, the combined facts that decomposition through $Li_2B_{12}H_{12}$ could result in H_2 pressure of practical interest and the fact that rehydrogenation of $Li_2B_{12}H_{12}$ is feasible suggest that the new phase of our research should be focused on the synthesis of $Li_2B_{12}H_{12}$ and its infusion into carbon to test whether $Li_2B_{12}H_{12}$ is formed in the dehydrogenation and can be rehyrogenated in a $LiBH_4$-carbon composite.

In Figure 5a, dehydriding of $LiBH_4$-carbon composite from room temperature to 300°C (1) as prepared composite, (2) second cycle of dehydriding after rehydriding at 300°C; 2,200 psig H_2 pressure; and (3) third cycle of dehydriding after rehydriding as in (2). The Y axis is with respect to total weight of the sample. The lack of low-temperature H_2 for Cycle 1 is possibly because of oxygen and moisture leakage into the sample during shipping. Although the increases in H_2 pressure in the region below 280°C were similar for the second and third cycle, there was evidence of some degradation in the storage property with further cycling as the pressure achieved at 300°C decreased noticeably in the third cycle. The low-temperature features in Cycles 2 and 3 are real because any solvent contaminant would have been pumped away after the first cycle.

After the third cycle at 300°C, the sample was subjected to two more dehydriding/rehydriding cycles in which the dehydriding was carried out to 350°C (at the end of this series, the sample would have been subjected to a total of five cycles, Figure 5b), and the rehydriding was also conducted at this temperature. The first dehydriding profile is shown in curve 4, and it appears to be quite similar to curve 3 of the previous slide. However, the dehydriding profile of the second cycle (curve 5) indicated further degradation of the H_2 storage property. After this series of experiments, the sample was subjected to four additional cycles of dehydriding/rehydriding with a temperature limit of 450°C. Within experimental error, all the dehydriding profiles (Figure 5b, curves 6-9) were the same and similar to curve 5. Steady and reversible performance has been attained.

Gao, et al., [1] proposed that a major reason for the loss in the reversibility in the hydrogen cycle for hydrides confined in carbon nanopores was due to the loss of alkali metals through reactions with carbon. They observed improved reversibility through the addition of alkali metals to the composite. Our data appear to support their proposal. After the third cycle at 300°C, the impurities on carbon that could react with the hydride at that temperature was depleted. Therefore, up to 300°C, the dehydriding profile of Cycle 4 did not deviate from that of Cycle 3 in any significant manner

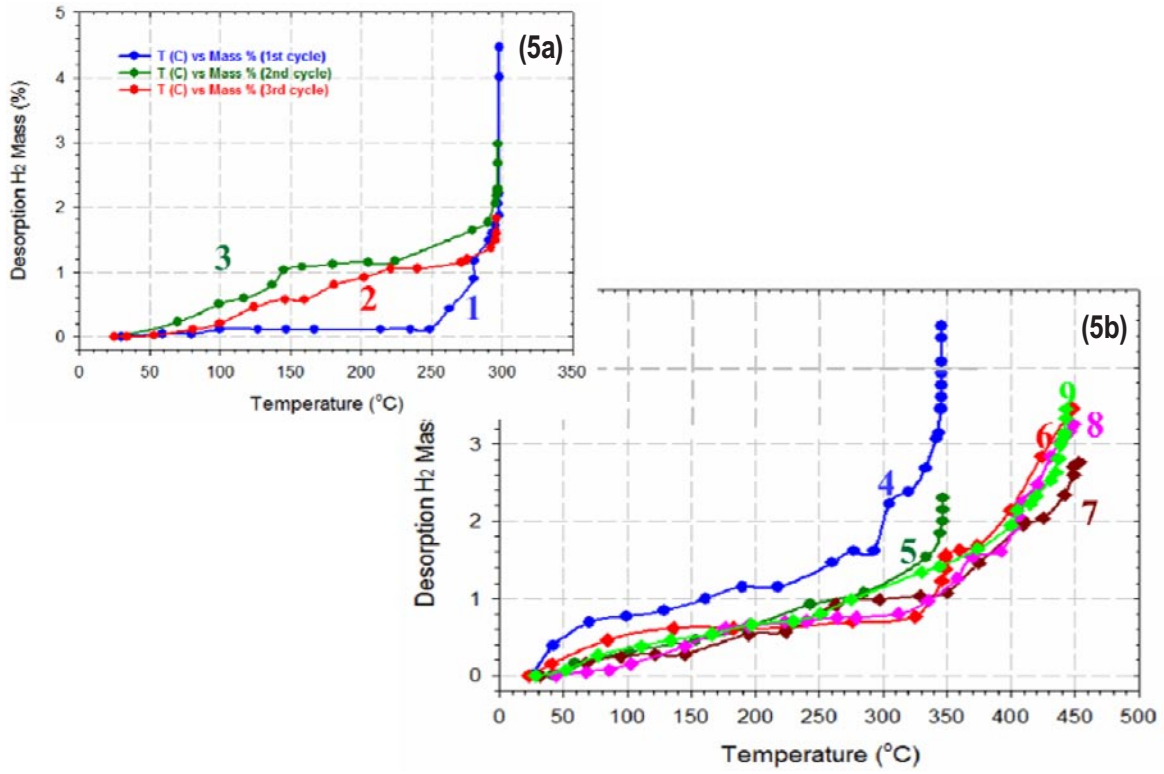

FIGURE 5. H_2 desorption of $LiBH_4$-carbon composite. The numbers indicate the cycle number of desorption. Hydrogenation temperature before desorption was 300°C for cycles 2-4; 350°C for cycle 5 and 450°C for cycles 6-9; pressure was at 2,200 psig.

(compare curve 4 and curve 3). However, cycle 4 terminated at 350°C, a temperature higher than any of the previous cycles, and as a result further reaction between the hydride and residual carbon impurities took place. This caused additional degradation in the amount of hydrogen released (curve 5). At this time, all reactive impurities on the carbon were depleted, and repeatable dehydriding profiles could be obtained, which were the last four cycles at 450°C. That reversible behavior can be obtained suggests that, indeed, the physical constraint of the carbon pores can suppress sintering.

NMR Studies of the Decomposition Products of $2LiBH_4+5Mg(BH_4)_2$

Multinuclear and high resolution magic angle spinning (MAS) solid-state NMR experiments were performed using a Bruker 500-MHz spectrometer and a Bruker 4-mm MAS probe (^{11}B background free). Samples include the as-milled mixture of 2:5 borohydrides and solid residue after H_2 desorption at lower temperatures. The ex situ ^1H and ^{11}B NMR spectra (Figure 6) showed eminent decrease of BH_4 (~ -41 ppm peak for both $LiBH_4$ and $Mg(BH_4)_2$) units and their transformation to other boron species. There was no single borane species (B_nH_m) that was identified unambiguously. The borane species were mainly characterized by a broad -26 ppm peak (see Figure 7) after thermal heating above 280°C.

Note that -26 ppm peak cannot be due to $Li_2B_{12}H_{12}$ of which resonance is expected at -15 ppm.

Besides the sharp -17.7 ppm and a broad peak at -1 ppm (amorphous boron), the main -26 ppm peak represents the major boron species. Considering all possible different boron bonding environments in B_nH_m, it is quite encouraging to see a single resonance to represent the desorption product.

Before the main -26 ppm peak, an ^{11}B peak at -30.5 ppm appeared upon heating at lower temperature (200°C). The peak could possibly be assigned to B_3H_8 formation. However, its formation was not in significant quantity, and other sharp peaks at -48.6 ppm and -17.8 ppm were accompanied. After heating at 200°C, the deduction in hydrogen content measured by ^1H NMR was less than 10% (Figure 8, [H] plot). [H] plot for the new batch showed noticeable difference from the first batch that contains boron oxide in large fraction.

The -48.6 ppm peak which might be transient, disappeared at higher temperatures. Such peaks at the high field are due to higher B coordination with more 3-center-2 electron bonds around B. Identifying such moiety could be valuable information in the early stage of the dehydrogenation reaction. The -17.7 ppm peak also formed at low-temperature heating, and remained unchanged up to 320°C. The -17.7 ppm peak can be associated with a stable boron species, such as closoborane, -15.5 ppm for $B_{12}H_{12}$. The

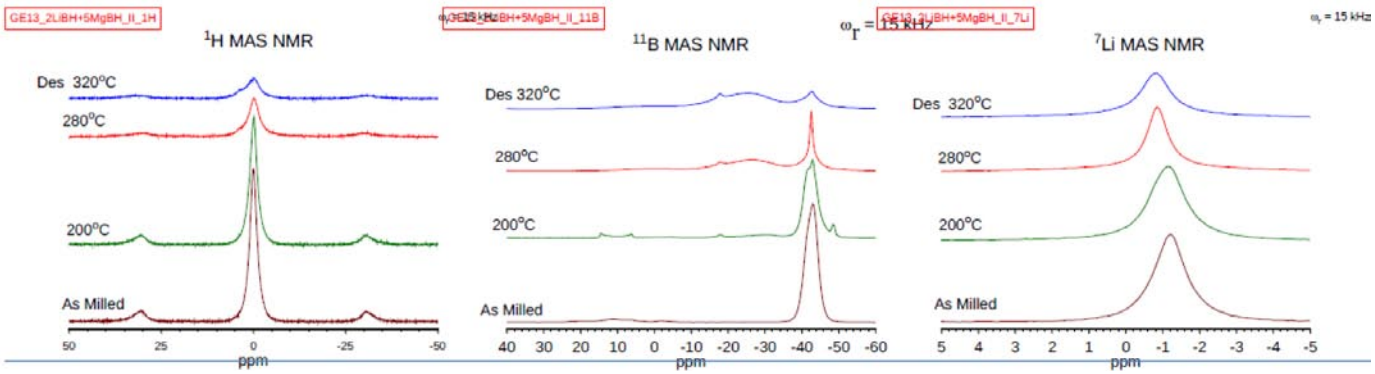

FIGURE 6. Solid-state NMR ^{1}H (left panel), ^{11}B (middle panel) and ^{7}Li (right panel) spectra upon H_2 desorption reactions.

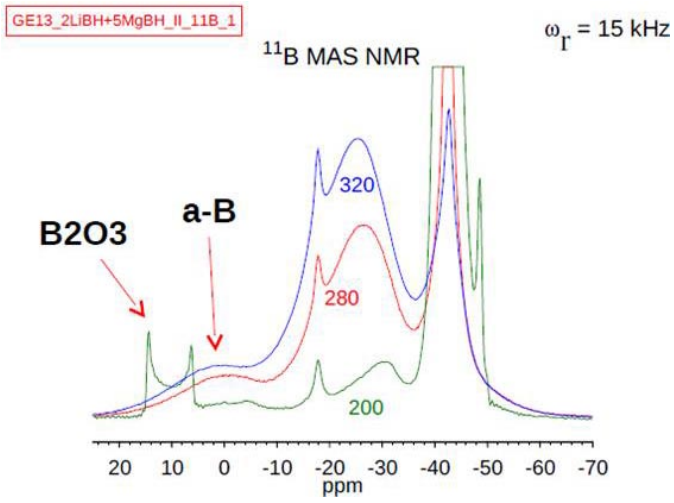

FIGURE 7. ^{11}B MAS NMR Spectra

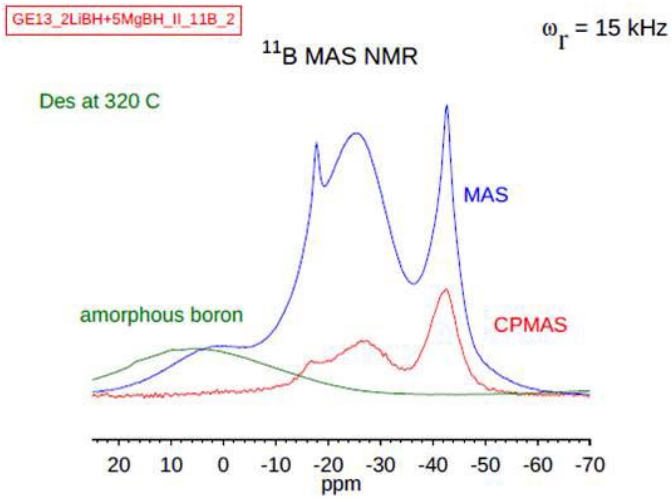

FIGURE 9. ^{11}B MAS NMR Spectra

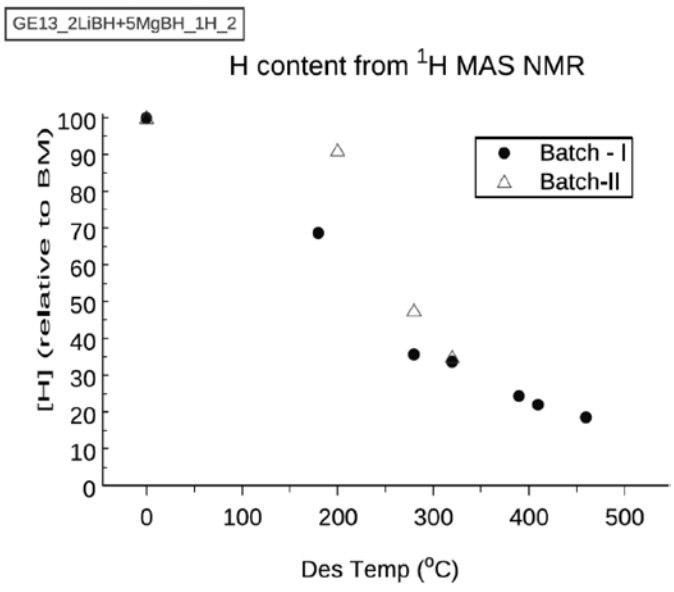

FIGURE 8. ^{1}H MAS NMR Using Two Batches

-26 ppm peak cannot be assigned to any known closo-borane structure although observing the single resonance is highly encouraging.

The peak near 0 ppm is assigned as amorphous boron at the moment. The peak appears at nearly the same position of the ^{11}B spectrum of neat amorphous boron (Aldrich). ^{1}H-^{11}B cross-polarization MAS NMR also supports the nature of the boron species which bears no direct B-H chemical bonds. It is surprising to see the formation of amorphous boron, because amorphous boron is not expected from the calculation (Figure 9).

Mass Transport in $Mg(BH_4)_2$ and $LiBH_4$

We have continued our study of mass transport in lithium borohydride ($LiBH_4$) and magnesium borohydride, $Mg(BH_4)_2$. Both materials exhibit high volumetric and gravimetric hydrogen densities and predicted thermodynamic properties that are promising for reversible onboard hydrogen storage, especially when used in destabilized reactions.

Thermodynamically, the dehydrogenation reactions in the pure compounds are predicted to take place as:

$$Mg(BH_4)_2 \rightarrow 1/6\ MgB_{12}H_{12} + 5/6\ MgH_2 + 13/6\ H_2 \quad (3)$$

$$LiBH_4 \rightarrow 1/12\ Li_2B_{12}H_{12} + 5/6\ LiH + 13/6\ H_2 \quad (4)$$

We have applied the model of mass transport to the reactions (3) and (4). This formalism is based on local equilibrium assumptions at interfaces where diffusion is driven by concentration gradients across the phases participating in the reactions. Defect formation energies are calculated from density-functional theory, and both charged and neutral defects are taken into account. Our results reported in the previous quarter show that neutral BH_3 vacancies in magnesium borohydride (BH_3) have the highest concentration gradient, while all other concentration gradients are several orders of magnitudes smaller. The structure of the neutral BH_3 vacancy is shown in Figure 10. It shows that removing a neutral BH_3 complex leaves behind a negatively charged H^- anion occupying the vacant site. The preferred diffusion mechanism involves an exchange of a neutral BH_3 complex with a near-neighbor BH_4^- anion as shown in Figures 10 and 11. Our density-functional theory results demonstrate that the calculated activation barrier is approximately 2 eV for $Mg(BH_4)_2$ and 1.6 eV for $LiBH_4$; both these values are significantly higher than the calculated migration barrier for AlH_3 vacancies in $NaAlH_4$ (0.34 eV). Together with the significantly lower (by several orders of magnitude) values of the vacancy concentration gradients when compared with those calculated by us for $NaAlH_4$; these results demonstrate that the intrinsic mass transport rates in magnesium borohydride and lithium borohydride are very slow due to the high energy barrier involved in forming the transition state structure with the doubly negatively charged BH_5 complex.

We will explore the effect of mixing Mg and Li borohydrides and the associated changes in diffusion rates due to the introduction of anion vacancies as a result of Mg^{2+}/Li^+ substitution in magnesium borohydride. This represents a promising strategy for accelerating mass transport and reaction kinetics in borohydrides.

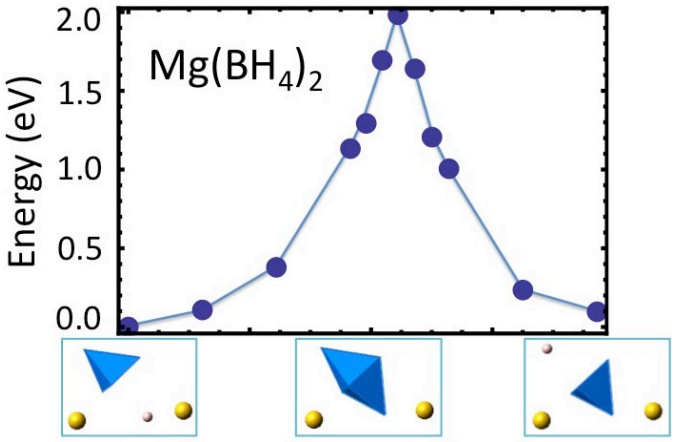

FIGURE 10. Calculated activation barrier for the diffusion of BH_3 vacancies in $Mg(BH_4)_2$. The H^- anion is colored pink, Mg^{2+} cations are yellow, and BH_n complexes are blue. Left panel shows the initial state with BH_3 vacancy on the lower left, the middle panel is the transition state, and the right panel shows the final state after BH_3 is exchanged between H^- and a neighboring BH_4^-.

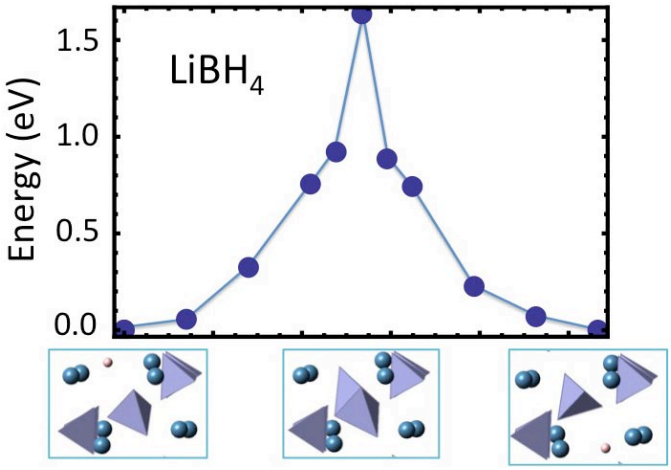

FIGURE 11. Calculated activation barrier for the diffusion of BH_3 vacancies in $LiBH_4$. Same convention as Figure 10, except Li^+ cations are blue.

FUTURE DIRECTIONS

- Complete synthesis of $B_{20}H_{16}$ (subcontract); perform desorption experiments for this compound; and extend NMR experiments to determine reaction products (if non-crystalline). Perform computations of observed reaction products to confirm results and provide predictions of thermodynamics/kinetics.
- Extend NMR experiments to "recharged" $2LiBH_4 + 5Mg(BH_4)_2$ samples, to determine portion(s) of the reaction that are reversible.
- Computational efforts to continue on kinetics, defects, diffusion/mass transport in promising predicted reactions (mass transport nearly complete; focusing on other barriers now – surface reactions, nucleation).
- Potentially promising avenue for "fast kinetics" borohydrides: low melting point combinations (i.e., low-lying eutectics). Direct some computational effort to finding these low-lying eutectics (*ab-initio* molecular dynamics and l-integration).
- Investigate the inclusion of various additives to $LiBH_4$-carbon composites 1) to improve the kinetics of the hydrogen cycle, 2) to ameliorate the initial degradation in cyclability, and 3) to influence the decomposition pathway so that $LiBH_4$ will decompose to more reversible reaction products.

REFERENCES

1. Gao, J.; Ngene, P.; Lindemann, I.; Gutfleisch, O.; de Jong, K.P.; de Jongh, P.E., Enhanced reversibility of H2 sorption in nanoconfined complex metal hydrides by alkali metal addition. *Journal of Materials Chemistry* **2012**,*22* (26), 13209-13215.